



Midlatitude surface temperature variability and teleconnection associated with warm and cold phases of El Niño/Southern Oscillation

Jai Hong Lee¹ · Pierre Y. Julien² · Seungho Lee³

Received: 28 October 2022 / Accepted: 5 June 2023

© The Author(s), under exclusive licence to Springer-Verlag GmbH Austria, part of Springer Nature 2023

Abstract

This study describes a comprehensive investigation of the contiguous US temperature patterns in relation to the warm and cold phases of El Niño/Southern Oscillation (ENSO) using a set of empirical and statistical analyses, such as harmonic analysis, annual cycle composites, and cross-correlation analysis. Monthly temperature composites for the first harmonic, covering 24-month ENSO events, are formed for all climate divisions over the USA spanning up to 29 ENSO episodes. From the harmonic vectorial maps plotted on the study area, each vector reveals both intensity and temporal phase of the ENSO-related temperature teleconnection, and the corresponding candidate and core regions are determined using a machine learning technique of a Gaussian mixture model (GMM) based on the magnitude and temporal phase of climate signal and Köppen climate classification. As a result of vectorial mapping, four core regions were designated as North-West/Central region (NWC), South-West region (SW), South-East region (SE), and North-East region (NE). During fall (0) to spring (+) seasons, the results of this analysis show positive (negative) temperature response to the El Niño events at the NWC region (SW, SE, and NE regions), while the opposite patterns are detected for the cold phase of ENSO. The temporal consistency values were 0.66 to 0.83 (0.77 to 0.86), and spatial coherence values ranged from 0.93 to 0.99 (0.95 to 0.99) for the El Niño (La Niña) events. Comparative analyses of temperature responses to both warm and cold ENSO events reveal the high significance level of the ENSO-temperature correlation with an opposite tendency in monthly temperature anomalies. Below normal temperature, anomalies during the El Niño thermal forcing are more significant than above normal temperature departures during the La Niña events. Consequently, middle-latitude temperature responses to the El Niño and La Niña phenomena are detectable over the contiguous USA.

1 Introduction

The El Niño/Southern Oscillation (ENSO) is a combined phenomenon of fluctuating sea surface temperature and atmospheric circulation over the central and eastern Pacific Ocean. It has a critical influence on climate patterns all over the world (WMO 2014). These large-scale naturally occurring phenomena have been investigated at regional

and global scale since the extreme phases of the ENSO episodes can cause major hydroclimatic extremes in various parts throughout the world. Many scientific approaches for understanding these phenomena have been providing us a chance to prepare for the disastrous hazards such as abnormal heat waves, severe cold weather, floods, and droughts.

Walker and Bliss (1923, 1932) studied firstly the impacts of the Southern Oscillation (SO) on the Indian hydroclimatic variability. Since then, a number of global-scale studies related to the ENSO extreme phases showed various notable climatic links between temperature patterns and either phase of these opposite extreme events in many areas throughout the globe. Since Berlage (1966) found that the ENSO extreme events correlated well with temperature anomaly on a global basis, Rasmusson and Carpenter (1983) related the temperature patterns to the extreme phase of Southern Oscillation and identified a significant link between the two

✉ Jai Hong Lee
june.lee@colostate.edu

¹ Department of Engineering, South Carolina State University, Orangeburg, SC, USA

² Department of Civil-Environmental Engineering, Colorado State University, Fort Collins, USA

³ South Carolina Lexington H. School, Lexington, SC, USA

variations. Also, Bradley et al. (1987) identified notable ENSO-related temperature signals using a set of high-quality temperature time series. They focused on the response of short-term fluctuations of continental surface air temperatures to the positive and negative phases of ENSO over the Northern Hemisphere. Halpert and Ropelewski (1992) investigated temporal and spatial ranges showing consistent response of the temperature pattern over a variety of areas throughout the world to the extreme phases of the ENSO episodes and showed significant correlations of the ENSO forcing and temperature patterns, which were also identified by Kiladis and Diaz (1989a, b). More recently, Daveyab et al. (2014) plotted global spatial maps categorizing the seasonality and location of typical land temperature responses to the El Niño events based on the rate of occurrence analysis results.

On a regional basis, many studies found plausible evidence of the ENSO far-reaching effect on the low and midlatitude climate variabilities as documented by van Loon and Madden (1981), Ropelewski and Halpert (1986), Kiladis and van Loon (1988), Kiladis and Diaz (1989a, b), and Redmond and Koch (1991). For midlatitude regions, several studies indicated the ENSO-related temperature correlation. For the Rocky Mountains area in the USA, van Loon and Madden (1981) described a significant stability of correlation between sea level pressure and the Southern Oscillation and surface air temperature in the northern winter. Ropelewski and Halpert (1986) studied the climatic links between the extreme Southern Oscillation and temperature anomalies over North America and showed the ENSO-related temperature signals. This finding was also confirmed by Kiladis and Diaz (1989a, b). They documented that during the warm phase of ENSO forcing below normal temperature, anomalies occurred in the southern USA. Kiladis and van Loon (1988) mapped composite surface temperatures over the Indian sector during the various stages of both high and low index phases of Southern Oscillation. Redmond and Koch (1991) employed the Southern Oscillation Index (SOI) as an indicator of the ENSO phenomena to examine the relationship between large-scale atmospheric circulation patterns and surface temperature in the western USA and concluded the Pacific northwest showed the greatest SOI-temperature correlations. Lee and Julien (2017, 2019b) showed teleconnection of the extreme phases of ENSO forcing and midlatitude temperature variability in the Korean peninsula, and Viet (2021) assessed the effects of ENSO on the temperature over the southern Vietnam region and developed a new ENSO index for the proposed area, i.e., southern Vietnam ENSO Index (VEI). Tamaddun et al. (2019) investigated the influence of ENSO forcing on the regional surface temperature over northern India during monsoon season and concluded that the warm episode years played a greater

role in causing temperature changes than the cold or neutral events. Kemarau and Ebo (2022) found that ENSO has a critical effect on temperature patterns over Kuching region in Malaysia with respect to Oceanic Niño Index (ONI) values. They used linear regression in predicting ENSO-related temperature anomalies and provided useful information for understanding the ENSO-temperature teleconnection in urban areas during the occurrence of ENSO.

Previous studies on the ENSO-related teleconnection have more focused on the warm phase of extreme events and the impacts of the cold phase of extreme events have less scientific attention since the latter is considered less distinct and causes less disastrous natural hazards than the former. There has been rare discussion in the literature about the teleconnections with a focus on comparative analysis and interpretation between the warm and cold phases of ENSO forcing. The present study examines the far-reaching effects of the two phases of ENSO on temperature anomalies in terms of degree of magnitude and temporal phase shift of the teleconnection. As described in the relevant literature, many previous studies concentrated on global- or rather broad regional-scale analyses. Despite the various researches on the ENSO-related climate teleconnection, little is known about the perspective of the ENSO forcing on the subregional temperature variability. Recently, extreme weather events are occurring in more localized and intensified areas and the corresponding hydrologic extremes have a devastating effect on people's lives, property, and the natural environment. Therefore, delving into the underlying influences of the extreme phases of climatic variation on various scopes of temperature patterns provides a constructive way to predict and prepare unexpected natural hazards. Thus, it is important to investigate systematically how the warm and cold phases of extreme ENSO events influence the subregional temperature patterns over the USA. Recently, more comprehensive information about spatial and temporal variability of hydrometeorological parameters is being asked by potential users of the climate information as they are modulated by the extreme phases of ENSO forcing. Prior literature investigated the teleconnection between the extreme phases of Southern Oscillation and temperature anomalies over the United States using the observational data from 1931 to 1980 period (50 years) covering only 11 ENSO episodes (Ropelewski and Halpert 1986). However, we recently experienced noticeably severe extreme ENSO episodes including strong El Niño events in 1982, 1997, and 2015 and strong La Niña events in 1988, 1999, 2010, and so on. This study is conducted to provide updated climate information of the temporal phase, spatial extent, and intensity of ENSO-related temperature signals at each of several locations over the proposed study area using updated long-term temperature data (1985–2020) spanning up to 29 ENSO episodes. In addition, from the perspective of methodological

approaches, the previous studies including Ropelewski and Halpert (1986, 1987) used a subjective zoning method for determining core regions based on visual inspection over the harmonic dial maps. This subjective graphical approach implies that the ENSO-related hydrometeorological variability may include some uncertainties caused by other factors. In the present study, to categorize more objectively the candidate and core regions associated with the extreme phases of the ENSO forcing, an AI (artificial intelligence) machine learning technique was employed for determining the ENSO-related temperature signal areas.

The main purpose of this study is to investigate temperature variabilities over the USA associated with two opposite phases of ENSO events (warm and cold phases) using composite and harmonic analyses. This study uses an improved description by temporal cycle and spatial outlook for the intensity, time shift, and areal boundary of the ENSO-temperature correlation. Also, the present study compares the two types of teleconnections induced by El Niño and La

Niña considering magnitude and trend of the significant responses, using annual cycle and cross-correlation analyses.

2 Data

The monthly temperature time series used in this study are based on 344 climate divisions covering all climate regions over the contiguous USA. The source of the applied dataset is the National Center for Environmental Information (NCEI) which is a governmental organization under the National Oceanic and Atmospheric Administration (NOAA). The NOAA monitors and operates the overall US meteorology. As shown in Fig. 1 and Table 1, the monthly climate division data cover the contiguous USA and range from 1895 to 2020 covering the overall ENSO episodes (29 El Niño and 22 La Niña). To identify a consistent far-reaching effect of ENSO events on temperature anomaly over the USA, two sets of extreme ENSO episodes are selected considering a comprehensive

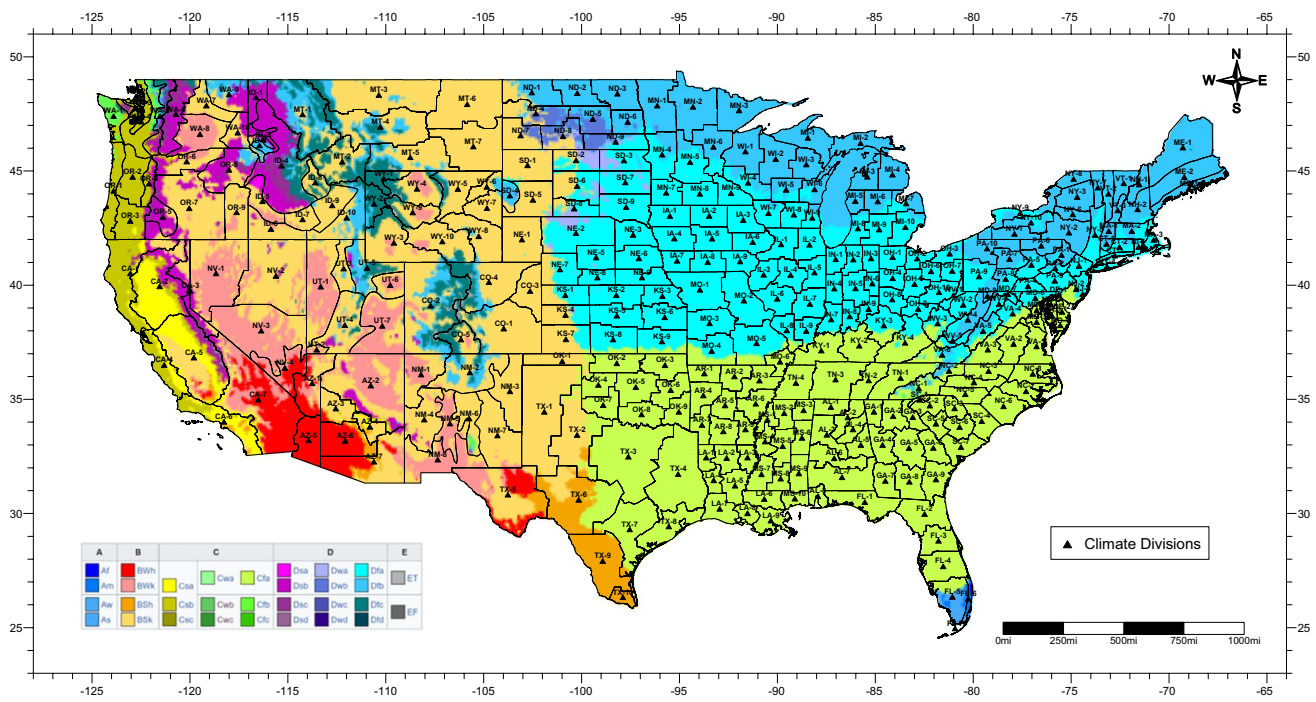


Fig. 1 Climate divisions and Köppen climate classification for temperature indices

Table 1 List of the ENSO episode years

El Niño years	La Niña years
1905, 1911, 1914, 1918, 1923, 1925, 1930, 1932, 1939, 1941, 1951, 1953, 1957, 1963, 1965, 1969, 1972, 1976, 1982, 1986, 1991, 1994, 1997, 2002, 2004, 2006, 2009, 2015, 2018	1910, 1915, 1917, 1924, 1928, 1938, 1950, 1955, 1964, 1971, 1973, 1975, 1985, 1988, 1995, 1998, 2000, 2005, 2007, 2010, 2011, 2017

scope of criteria defined by Ropelewski and Halpert (1987, 1989), Rasmusson and Carpenter (1983), Kiladis and Diaz (1989a, b), and Lee et al. (2019a). The ENSO years for the two phases of extreme events selected in the present analysis are listed in Table 1. The SOI is applied as an indicator of representing large-scale climate variation over the central-eastern Pacific Ocean (ENSO). This present analysis applied the SOI data calculated and recorded by the NOAA Climate Prediction Center. These SOI time series are computed based on the difference of the standardized sea level pressure (SLP) anomaly between Tahiti and Darwin, Australia.

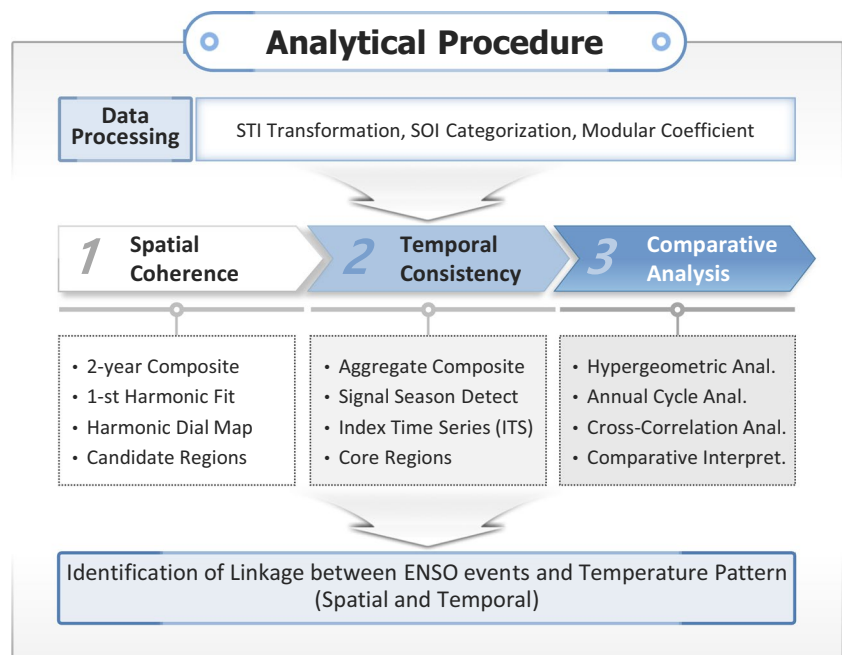
3 Method

To examine the spatiotemporal extent to which El Niño/La Niña affects temperature patterns over the USA, an empirical method (Ropelewski and Halpert 1986), annual cycle and cross-correlation analyses, is employed with some changes and additions. As shown in Fig. 2, the specific procedure of this analysis consists of mainly three steps, namely, data processing, spatial and temporal analyses, and comparative statistical assessment. In the first step, the original raw data are transformed into appropriate data formats, e.g., ranked percentile, modular coefficients, and categorized SOIs (Ropelewski and Halpert 1986; Jin et al. 2005). In the second step, candidate and core regions are determined using composite and harmonic analyses (Ropelewski and Halpert 1986; Lee and Julien 2016). Then, in the last step, El Niño/

La Niña-related temperature signals are compared using lag cross-correlation and annual cycle analyses.

Monthly temperature data of 344 climate divisions over the USA are fitted to probability density functions for calculating the Standard Temperature Index (STI) using a standardized method developed by McKee et al. (1993). The fitted distribution can be transformed into a cumulative density function (CDF) of the standard normal distribution by the equal-probability conversion technique as shown in Fig. 3. The STI time series, which have a mean of zero and standard deviation of unity, are used in the composite and harmonic analyses. Monthly temperature time series are transformed into modular coefficients for carrying out annual cycle analysis. These modular coefficients remove the effects of dispersed variance and mean values. The temperature data are expressed as percentages for the annual mean values. The modular coefficient data are calculated by the rate of each monthly temperature value to the monthly average value for the entire data. It places all divisions on the same cycle with unchangeable condition of the cyclic feature of the values at the same time. In this present study, lag cross-correlation coefficients are computed for temperature data and categorized SOI time series on a seasonal basis. To do this, four seasonal temperature and SOI time series are formed by averaging 3-month values. The four seasons consist of December–February (DJF), March–May (MAM), June–August (JJA), and September–November (SON). Then, all SOI values are categorized into five levels based on the magnitudes of individual data (Jin et al. 2005). The five categories of the SOI values are strong warm phase, weak warm phase, normal phase, weak cold phase, and strong cold

Fig. 2 Flowchart of the empirical methodology



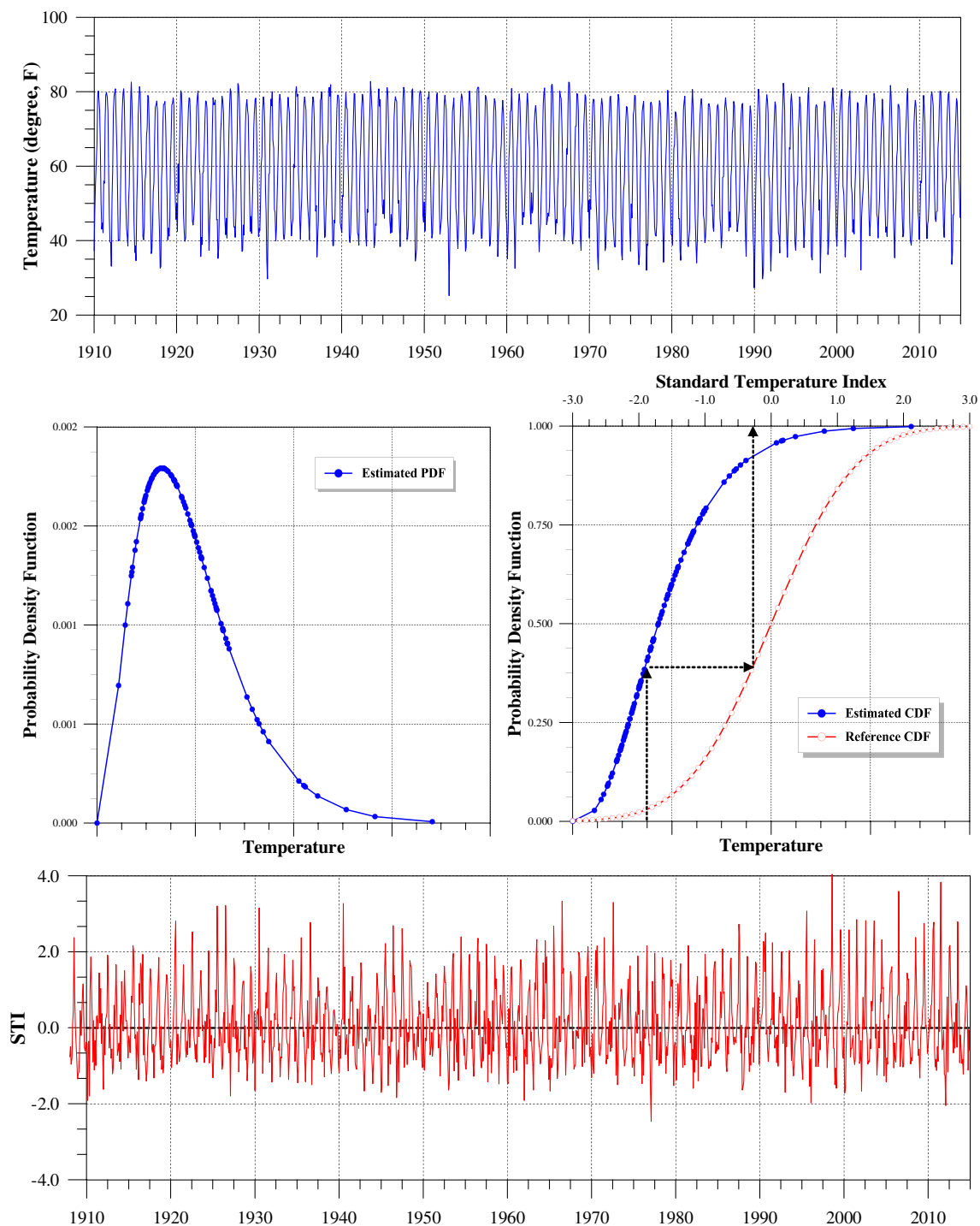


Fig. 3 STI estimation

phase. On the other hand, the seasonal temperature data are converted into percentile ranked probability time series to remove periodicities in temperature time series and to deal with the disparities among climate divisions. The percentile ranked probability values are based on Weibull plotting

position formula. All temperature values are ranked in an ascending order and then divided by $n + 1$ (n , size of data).

Monthly temperature composites on 24-month basis are computed for each climate division, starting with the July preceding the event, continuing through the June following the event year, for both high and low phases of the SO. The

July preceding the event is designated as Jul (−), while the June following the event year is expressed as Jun (+). Composites are computed separately for each phase of the SO. The composite for each climate division is then fitted with the first harmonic of an idealized 24-month SO cycle (either warm or cold episodes). This method assumes one temperature peak (or trough) during the duration of an SO event and that the SO is phase locked to the annual cycle. A 24-month compositing period was chosen since this defines the period during which one phase of the SO goes through its entire cycle (Rasmusson and Carpenter 1983). In the first harmonic cycle, the amplitude represents magnitude of the ENSO-related temperature signals, and the angular phase indicates time of the peak anomaly from the mean value (Fig. 4). The formula of the harmonic fits is as follows (Wilks 1995):

$$y_t = \bar{y} + \sum_{i=1}^{n/2} \left\{ C_i \cos \left[\frac{2\pi it}{N} - \beta_i \right] \right\}$$

$$= \bar{y} + \sum_{i=1}^{n/2} \left\{ A_i \cos \left[\frac{2\pi it}{n} \right] + B_i \sin \left[\frac{2\pi it}{n} \right] \right\}$$

$$A_i = \frac{2}{n} \sum_{t=1}^n y_t \cos \left(\frac{2\pi it}{n} \right), B_i = \frac{2}{n} \sum_{t=1}^n y_t \sin \left(\frac{2\pi it}{n} \right), C_i = (A_i^2 + B_i^2)^{0.5}$$

$$\beta_i = \tan^{-1} \frac{B_i}{A_i} (A_i > 0), \frac{\pi}{2} (A_i = 0), \tan^{-1} \frac{B_i}{A_i} \pm \pi (A_i < 0)$$

where y_t is monthly temperature value, \bar{y} is the mean temperature value, t is time of observation, i is number of harmonic fits, n is sample size, C_i is amplitude of the harmonic curve (magnitude of curve), β_i is time of harmonic peak (temporal phase of curve), and A_i and B_i are Fourier coefficients.

After the climate division composites are fit with a 24-month harmonic, the amplitude and phase of the curve is plotted as a vector for each station. In the analysis convention chosen here, the vector points toward the positive part of the cycle, that is, warmer-than-normal temperature. It is only after examining the composites, described below, that the actual sign of the SO-temperature relationship can be determined. This study is concerned with regional areas of the USA that exhibit strong SO-temperature relationships over periods of many months. Therefore, individual, or isolated, climate division that shows strong apparent relationships or areas that have short-time scale relationships is not considered for further study.

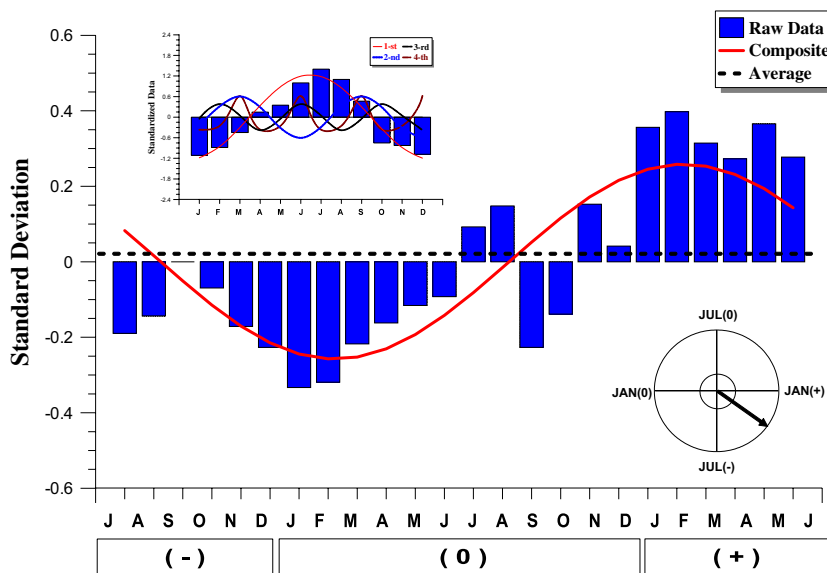
Plotting the harmonics as vectors on a map provides a method to spatially identify candidate geographic areas that appear to have a coherent ENSO response. We attempted to choose the largest areas of coherent ENSO response, where the “coherence” is estimated through the computation of the ratio of the magnitude of the average vector to the arithmetic average value of the vector magnitudes.

$$SC = \frac{\left[(\sum V \cos \theta)^2 + (\sum V \sin \theta)^2 \right]^{1/2}}{\sum V}$$

where the numerator is the average vector magnitude of all harmonic vectors within the candidate regions, the denominator is the arithmetic average value of the vector magnitudes, θ is angle of the vector, and V is magnitude of the vector.

The analysis that follows is limited to areas for which values of the coherence were equal to or greater than 0.80 (Ropelewski and Halpert 1986; Lee and Julien 2018). This eliminates from the analysis regions that contain harmonic

Fig. 4 A first harmonic fit to the temperature ENSO composite for the climate division SC-5. The amplitude and the phase of the first harmonic are presented as a harmonic dial (the lower right). The inset diagram (the upper left) depicts an example illustrating several harmonic fits of annual cycle for monthly temperature from the first to the fourth harmonic



vectors with large amplitudes at a few stations which have little consistency in phase, i.e., low coherence. Aggregate composites are formed to detect the ENSO-related temperature signal seasons. These signal seasons represent apparently consistent temperature responses to the extreme ENSO forcing. All ENSO composite values in a candidate region are averaged and plotted on a 24-month period to cover the entire ENSO cycle and identify accurately the signal season. One season within the aggregate composite is found by detecting a group of values showing more than five consecutive months with the same sign. The event year and the following year are regarded as the responding period of ENSO phenomena, considering the distance between the study area in midlatitude and the ENSO area in the Pacific Ocean. Index time series (ITS) are computed by temporally averaging temperature values of the signal seasons for the entire years of record and by spatially averaging the temperature data over the candidate regions. The ITS values are used to quantify the temporal consistency of the ENSO impact on temperature patterns. Temporal consistency rates for the candidate regions are computed using the rate of the number of years exhibiting ENSO signal in ITS to the number of all ENSO event years. These temporal consistency rates are the determinant of the core regions showing consistent temperature responses to ENSO phenomena. In addition, extreme temperature events are examined in association with ENSO forcing as demonstrated by Ropelewski and Halpert (1986). They investigated climate linkage between ENSO events and extreme temperature occurrences. In the present study, the number of years showing the ENSO-related extreme temperature signal is counted during the signal season. To assign the highest and lowest levels of the extreme events, the ITS time series are ranked from the highest value to the lowest value, normalized by the entire data, and transformed to the probability time series (Kahya and Dracup 1994). The highest value is assigned to the probability of 80% ITS, while the lowest value is assigned to the probability of 20% ITS.

A machine learning technique, Gaussian mixture model (GMM), was employed for diminishing the degree of subjectivity when candidate regions were determined based on the magnitude and temporal phase of the ENSO-related temperature signals. GMM algorithm is based on a statistical learning technique used in identifying a subset of discrete data which represent a feature space. As a measurable characteristic, the feature can describe phenomena being observed and the corresponding feature data can form a feature space by defining collectively the single or multidimensional range. For the purpose of classifying the candidate regions objectively, three features are selected in this study, i.e., the intensity of the ENSO-related temperature teleconnection, temporal cycle of each temperature response, and Köppen climate classification. All harmonic dial vectors fall somewhere in the feature space. The GMM method takes

advantage of a probability model instead of objective functions of distance measurements as opposed to the commonly used clustering techniques, e.g., fuzzy *C*-means or *k*-means, which are based on distance measures. In the GMM algorithm, each cluster is classified by a parametric probability density based on a mixture model of probability distribution followed by dataset, and the cluster structure is modeled by finite mixture. Although the GMM technique has been considered a powerful tool for cluster analysis in many research fields, there has been little attention to its practical application in hydroclimatological studies. The dimension of the input data affects largely the results of cluster analysis because the GMM is based on the probability model. Therefore, it is of great importance to select appropriate feature subset for conducting cluster analysis. Multivariate distribution of a given dataset can be fitted with a normal mixture model for cluster structure. Multivariate data, y_n , which is composed of m independent samples with variables, comprises C clusters in the dataset, and a probability distribution is assigned to each sample with a density function. Mixture probability density function, pdf, is weighed for the densities of C clusters as follows:

$$\text{pdf}(y_n|\beta) = \sum_{i=1}^C p_i h_i(y_n|\mu_i, V_i)$$

where p_i is mixing proportions, h_i is normal probability density function, μ_i is mean of h_i , and V_i is variance matrix. If an indicator vector of y is $d = [d_1, \dots, d_m]$ with $d_m = [d_{n1}, \dots, d_{ni}]$, the mixture model log likelihood is as follows:

$$L(\beta|y_1, \dots, y_m, d_{ni}) = \sum_{n=1}^N \ln \left[\sum_{i=1}^C d_{ni} p_i h_i(y_n|\mu_i, V_i) \right]$$

Also, the parameter $\beta = (p_1, \dots, p_i, \mu_1, \dots, \mu_i, V_1, \dots, V_i)$ can be selected for maximizing the log-likelihood. Here, many normal mixture models can be chosen according to the geometric features of each cluster that includes the expression of the cluster variance matrix.

Hypergeometric distribution test is employed to assign the significance level of the ENSO-temperature correlation. Haan (1977) conducted the hypergeometric distribution test calculating “the cumulative probability that at least m successes are obtained in n trials from a finite population of size N containing k successes.” A cumulative probability computed from the hypergeometric distribution gives an occurrence significance level of the relationship previously defined for both extreme phases of the ENSO. Kahya and Dracup (1994) used hypergeometric test in terms of average value and high-low extreme events. In the present test, two cases (I and II) are considered according to the definition of a success. In case I, a success is defined as the occurrence

of years that an ITS value associated with ENSO events is higher (lower) than the median, while in case II, a success is defined as the occurrence of year in which an ITS value associated with ENSO events falls into the upper (lower) 20% of the distribution. Annual cycle analysis is used as a comparative interpretation of two ENSO effects on the temperature anomaly from the perspective of magnitude and annual trend of the signal. Monthly temperature time series are transformed into modular coefficients for carrying out annual cycle analysis. These modular coefficients remove the effects of dispersed variance and mean values. The temperature data are expressed as percentages for the annual mean values. The modular coefficient data are calculated by the rate of each monthly temperature value to the monthly average value for the entire data. These annual cycle plots make it possible to determine whether the extreme phases of warm and cold ENSO events modulate temperature increasingly or decreasingly. Cross-correlation coefficients are calculated on a seasonal basis to compare the positive and negative ENSO-related temperature signals. Five categorized SOI datasets as ENSO index are correlated with the monthly temperature time series expressed by percentile ranked probability. The resulting correlation coefficient values indicate the magnitude and sign of the relationship between the temperature patterns and the ENSO forcing on a seasonal basis. A more detailed explanation of the data conversion and correlation procedure was described in the first section of data processing.

4 Results

4.1 El Niño–temperature relationship

Figure 5 shows the harmonic dial map with the detected candidate regions from the results of composite and harmonic analyses. The vectorial map for temperature indicates four regions of the USA that appear to have a coherent ENSO response. The candidate regions are the North-West/Central region (NWC), the South-West region (SW), the South-East region (SE), and the North-East region (NE). As shown in Table 2, composite temperature indices for each region indicate that the NWC, SW, SE, and NE regions may have an ENSO-related response. The temperature composites for the four candidate regions show clearly defined cold and warm seasons within the ENSO cycle, and thus, they are explained in detail for further consideration in this analysis.

The North-West region (NWC) includes 49 climate divisions, extending from Washington and northern Oregon to northern Wisconsin and Michigan and including all of Montana and North Dakota and northern South Dakota and Minnesota. The time series of the November (0) to May (+) temperature indices averaged over all

climate divisions in the NWC region (Fig. 6) illustrates the notable consistency in the temperature with respect to the ENSO in this part of the USA. This season showed above normal, i.e., higher than the average temperature for 24 out of 29 ENSO events. Further, of the 25 occurrences of index values equal to or higher than the highest ITS limit (80%), 13 of them occurred in association with ENSO. Two of the occurrences in the lowest ITS limit (20%) were associated with ENSO. The spatial coherence and temporal consistency were 0.97 and 0.83. The South-West region (SW) occupies all of California, Nevada, Utah, Arizona, Colorado, New Mexico, and parts of Kansas, Oklahoma, and Texas. The time series of the SW region temperature index based on the climate division data for the October (0) to April (+) season (Fig. 7) shows below normal temperature for 21 out of the 29 ENSO events. While the index shows values of lower than or equal to the lowest ITS limit (20%) for 13 of the ENSO years, negative values of the same magnitude or smaller also occur during 10 non-ENSO-related years. Only one of the ENSO-related seasons in the SW area falls into the highest ITS limit (80%). The spatial coherence and temporal consistency were 0.93 and 0.72. The South-East region (SE) covers 80 climate divisions and includes all of Florida, South Carolina, Georgia, Alabama, Mississippi, Louisiana, Arkansas, Tennessee, part of North Carolina, and almost all of Texas and Oklahoma. The time series of the November (0) to May (+) temperature indices averaged over all stations in the SE region (Fig. 8) illustrates the notable consistency in the temperature with respect to the ENSO in this part of the USA. This season showed below normal, i.e., lower than the average temperature for 21 out of 29 ENSO events. Further, of the 25 occurrences of index values equal to or lower than the lowest ITS limit (20%), 10 of them occurred in association with ENSO. Three of the occurrences in the highest ITS limit (80%) were associated with ENSO. The spatial coherence and temporal consistency were 0.99 and 0.72. The North-East region (NE) has the smallest area containing 42 climate divisions and covers part of Kentucky; almost all of North Carolina, West Virginia, and Pennsylvania; and all of Maryland, Delaware, and New Jersey. The time series of the NE region temperature index based on the climate division data for the October (0) to March (+) season (Fig. 9) shows below normal temperature for 19 out of the 29 ENSO events. While the index shows values of lower than or equal to the lowest ITS limit (20%) for 8 of the ENSO years, negative values of the same magnitude or lower also occur during 13 non-ENSO-related years. Only two of the ENSO-related seasons in the NE area fall into the highest ITS limit (80%). The spatial coherence and temporal consistency were 0.98 and 0.66.

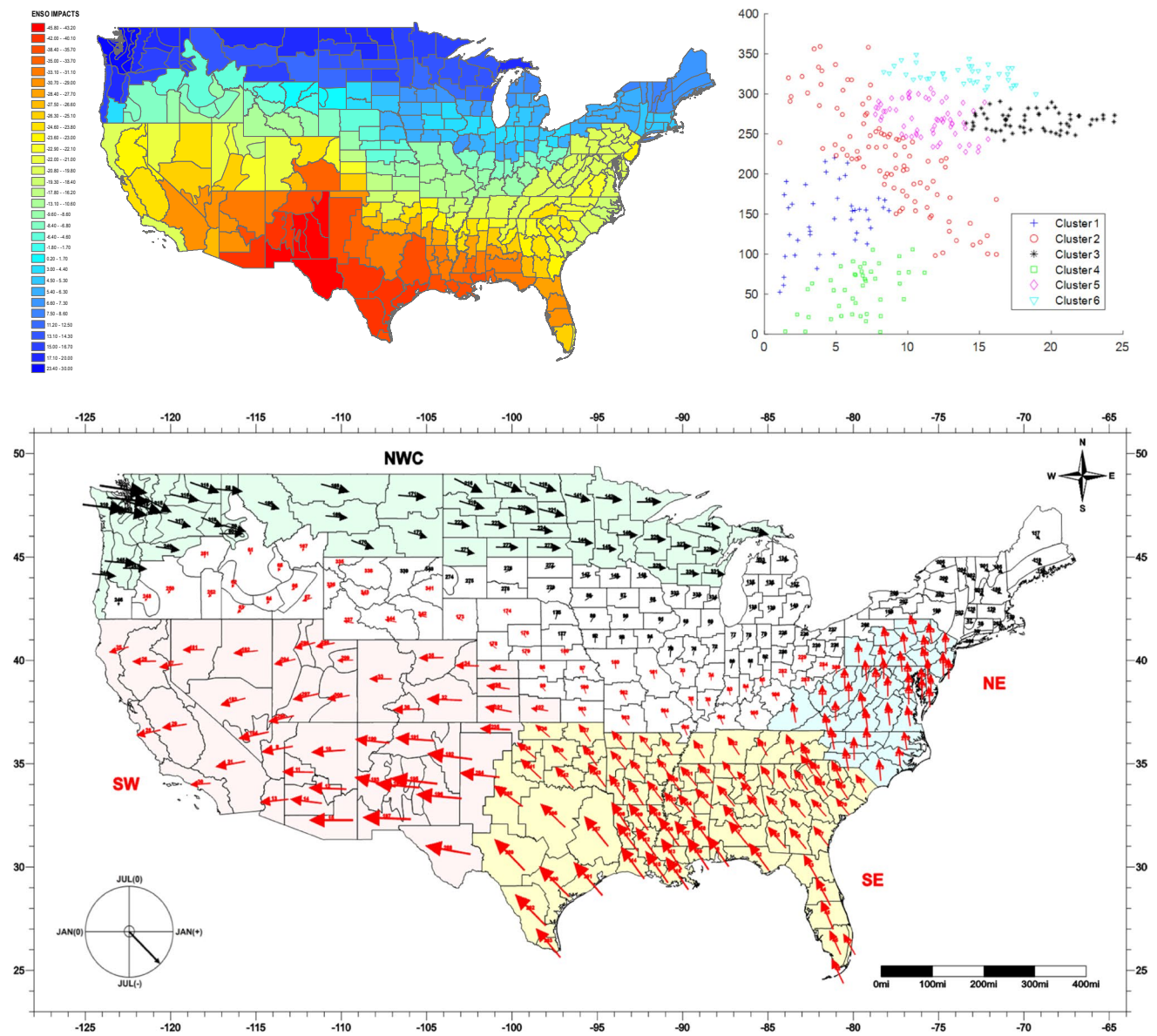


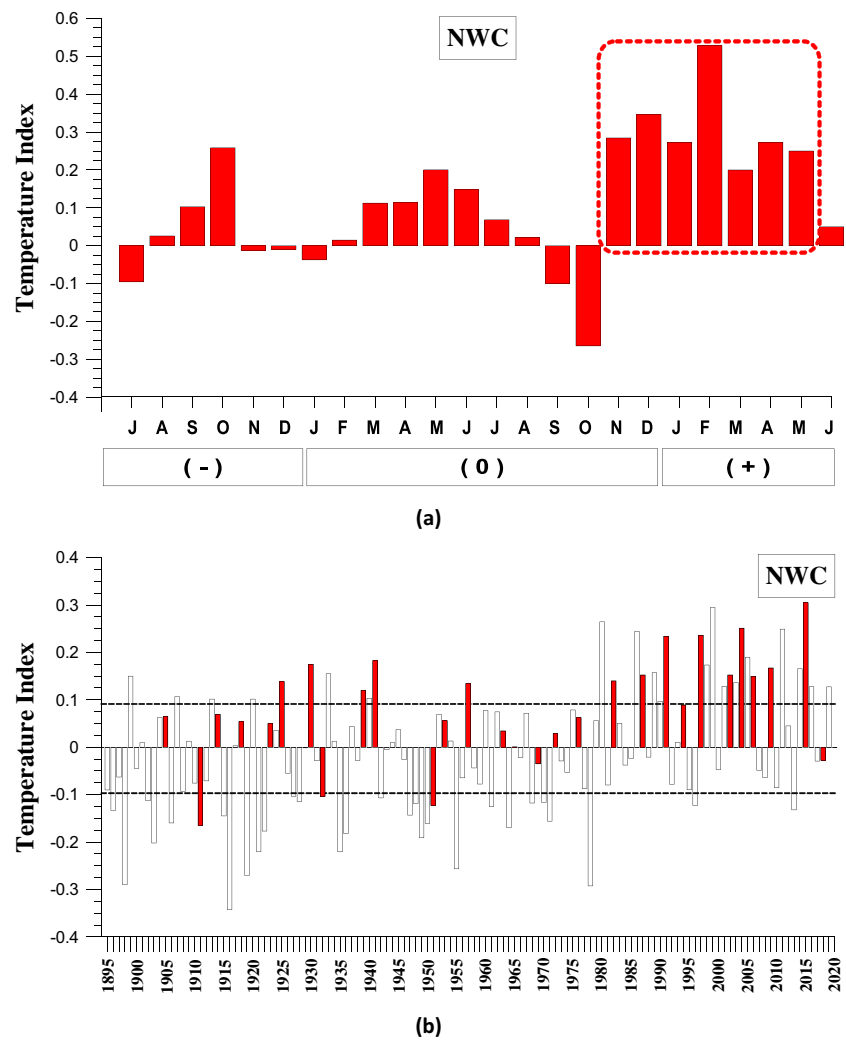
Fig. 5 Image map (upper left), clustering results (upper right), and harmonic dial map (lower) based on the first harmonic of the 2-year El Niño composites. In the image map, the blue areas indicate positive response of temperature anomalies to ENSO forcing, while the red areas indicate negative ENSO-related temperature signals. The

NWC region shows positive responses, while the SW, SE, and NE regions show negative responses. In the harmonic dial map, scale for the direction of arrows: south, July (–); west, January (0); north, July (+); and east, January (+). The magnitude of arrows is proportional with the amplitude of the harmonics

Table 2 Properties of the candidate regions (El Niño events)

Region	Season	Coherence	Total episode	Occurrence episode	Consistency	Extreme events
NWC	Nov (0)–May (+)	0.97	29	24	83%	13
SW	Oct (0)–Apr (+)	0.93	29	21	72%	13
SE	Nov (0)–May (+)	0.99	29	21	72%	10
NE	Oct (0)–Mar (+)	0.98	29	19	66%	8

Fig. 6 **a** El Niño aggregate composite for the candidate NWC region. The dashed line box delineates the season of possible El Niño-related responses. **b** The index time series for the NWC region for the season previously detected. El Niño years are shown by solid bars. The dashed horizontal lines are the upper (80%) and lower (20%) limits for the distribution of ITS values

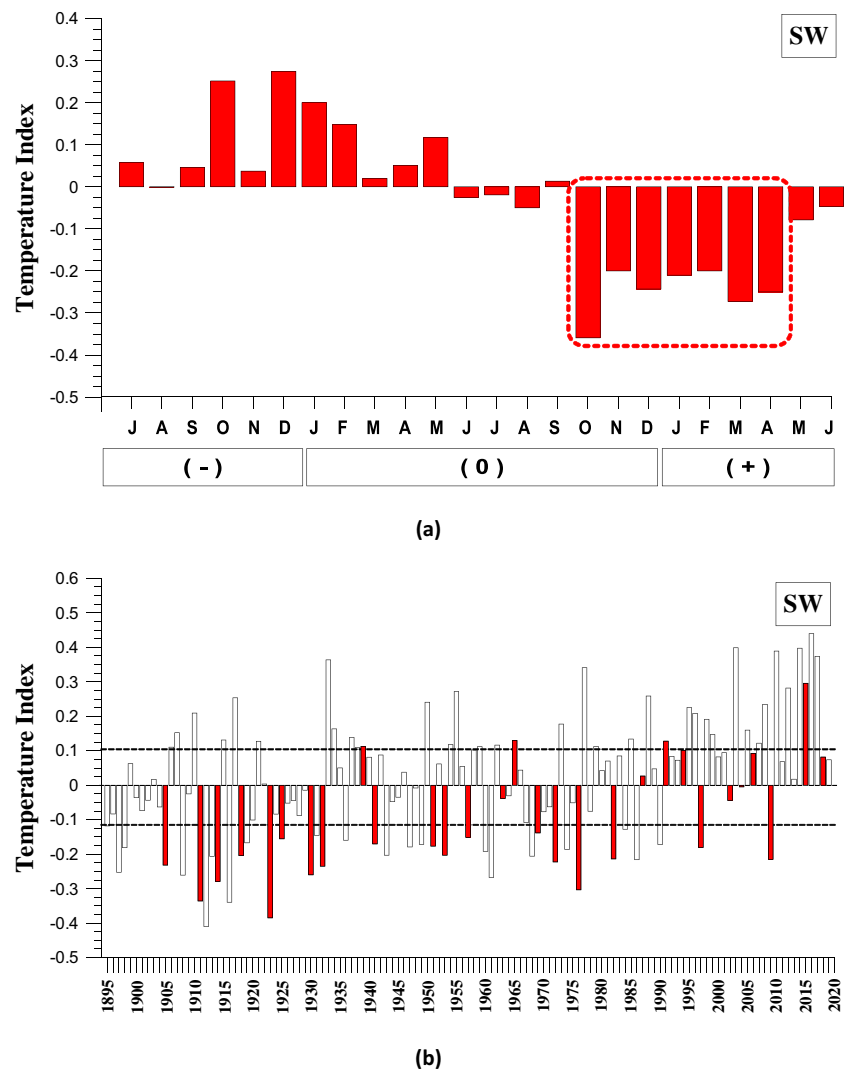


4.2 La Niña–temperature relationship

For 22 La Niña episodes, which are the cold phase of ENSO, the composite and harmonic analyses were performed on the monthly temperature data. The resulting map of harmonic dial vectors (Fig. 10) indicates coherent responses within the four outlined regions, the North-West/Central region (NWC), the South-West region (SW), South-East region (SE), and North-East region (NE). ENSO composites of temperature indices for each of the regions (Figs. 11, 12, 13, and 14) indicate that the four regions have well-defined seasons of potentially significant ENSO-related response. The overall results of the composite and harmonic analyses are outlined in Table 3.

The North-West/Central region (NWC) includes 48 climate divisions, extending from Washington to northern Michigan and including all of North Dakota, Minnesota, and Wisconsin; northern Montana; and part of Idaho and South

Dakota. The time series of the standardized temperature departure averaged over the all climate divisions in the NW region for the November (0) to June (+) season (Fig. 11) show negative temperature departure for 17 out of 22 ENSO events. The index values equal or exceed the lowest ITS limit (20%) in 8 of the ENSO years. None of the occurrences in the highest limit (80%) was associated with ENSO. The spatial coherence and temporal consistency were 0.99 and 0.77. The South-West region (SW) includes all of California, Nevada, Utah, Arizona, Colorado, New Mexico, and Texas and western Kansas and Oklahoma. In the SW region, the apparent ENSO-related temperature response occurs in October (0) to June (+). The time series of spatially averaged standardized temperature departures for this season (Fig. 12) shows positive departures for 19 out of 22 ENSO events. The index shows values of higher than or equal to the highest ITS limit (80%) for 10 of the ENSO years. None of the ENSO-related seasons in the SW area fall into the

Fig. 7 As in Fig. 6, except for the candidate SW region

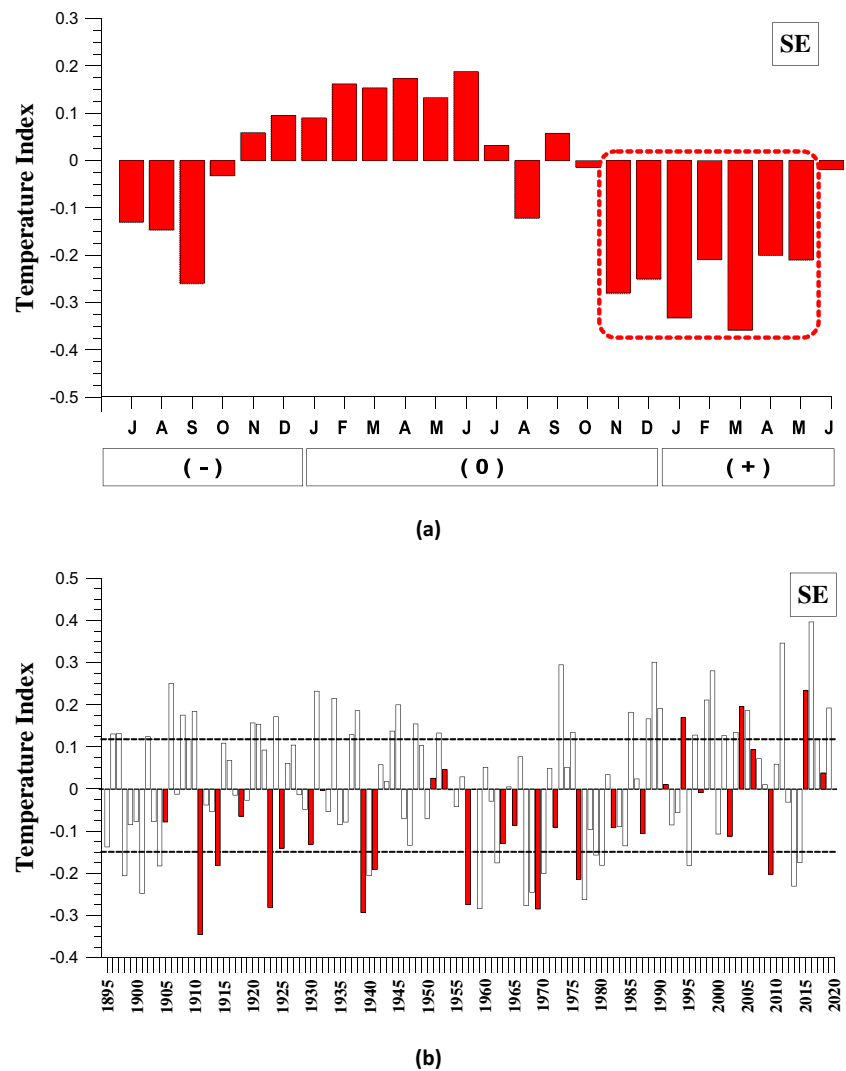
lowest ITS limit (20%). The spatial coherence and temporal consistency were 0.98 and 0.86. The South-East region (SE) covers 64 climate divisions, and includes all of Florida, South Carolina, Georgia, Alabama, Mississippi, Louisiana, Tennessee, and part of North Carolina. The time series of the standardized temperature departure averaged over the all climate divisions in the SE region for the October (0) to May (+) season (Fig. 13) show positive temperature departure for 17 out of 22 ENSO events. The index values equal or exceed the highest ITS limit (80%) in 8 of the ENSO years. None of the occurrences in the lowest limit (20%) was associated with ENSO. The spatial coherence and temporal consistency were 0.96 and 0.77. The North-East region (NE) has the smallest area containing 30 climate divisions and covers part of Kentucky, Pennsylvania, almost all of North Carolina and West Virginia, and all of Maryland and Delaware. In the NE region, the apparent ENSO-related temperature response occurs in October (0) to March (+). The time series of

spatially averaged standardized temperature departures for this season (Fig. 14) shows positive departures for 18 out of 22 ENSO events. The index shows values of higher than or equal to the highest ITS limit (80%) for 8 of the ENSO years. One of the ENSO-related seasons in the NE area falls into the lowest ITS limit (20%). The spatial coherence and temporal consistency were 0.95 and 0.82.

4.3 Comparative analysis of El Niño and La Niña

The probability that warm (cold) season occurs at random during the ENSO event years was tested by the hypergeometric distribution. In case I, the application of the hypergeometric distribution model results in a very low level of probability of occurrence by chance (less than 0.04) for both events. In case II, the probability is also very low for both phases of extreme events except for the NE region for the El Niño events. The extreme temperature conditions appear to be almost exclusively related to ENSO events

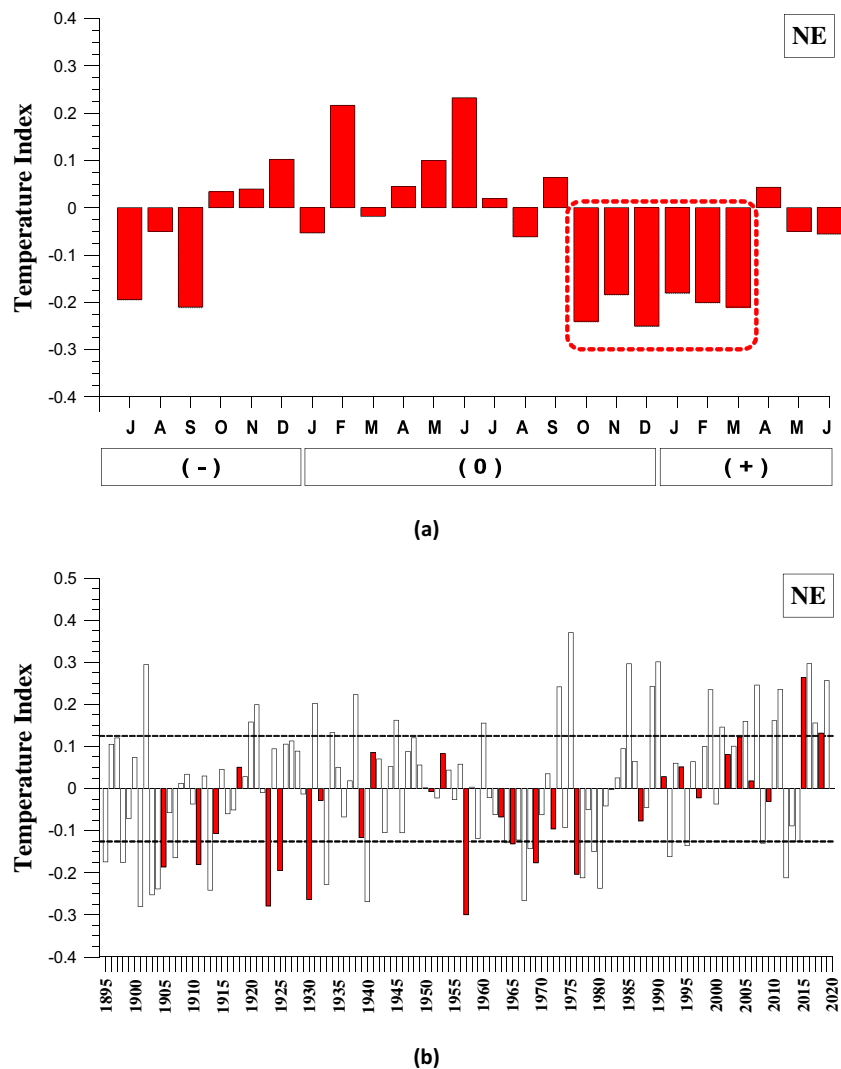
Fig. 8 As in Fig. 6, except for the candidate SE region



in the 125-year period. Overall results in Tables 4 and 5 are also consistent with the high confirmation rates (66–83% for El Niño events and 77–86% for La Niña events) for temporal consistency of the signals. All of this implies that the relationship depicted in the aggregate composites is probably due to nonrandom forcing mechanism, i.e., the tropical thermal anomalies. Monthly temperature time series are transformed into modular coefficients for carrying out annual cycle analysis. From this resulting series, El Niño and La Niña composites are formed and plotted along with the regional annual cycle (Figs. 15 and 16). Examination of these figures reveals two fundamental features. First, for a typical temperature behavior during El Niño events, the NWC (SW, SE, and NE) showed an enhanced (suppressed) temperature of the annual cycle from the end of event year to the beginning of the following year. Second, for typical temperature behavior during La Niña events, the NWC (SW, SE, and NE) showed a decreased (increased) amplitude from the end of the event

year to the beginning of the following year. This enhancement and suppression of magnitudes are roughly concurrent with the previously detected warm and cold signal seasons in four core regions. Also, an opposite tendency in monthly temperature fluctuations between the El Niño and the La Niña composites during a 24-month period is noticeable. In summary, the resulting findings suggest that the tropical heating (cooling) anomalies modulate the annual temperature cycle within the USA by increasing (decreasing). Table 6 displays the results of calculating cross-correlation coefficients. These values represent intensity and sign of the correlation between the ENSO phenomena and temperature anomalies. This correlation analysis is conducted for large-scale climate indicator (ENSO index) and the seasonal temperature anomalies, which use five categorized SOI datasets and percentile ranked probabilities, respectively. As a result, the seasonal temperature anomalies were significantly correlated with both extreme phases of SO at 0.05 significance level. The highest

Fig. 9 As in Fig. 6, except for the candidate NE region



positive correlation coefficient values are shown in the lag-0 to lag-2 cases over the NWC region, and negative correlations are found in the lag-0 to lag-2 (lag-1 to lag-3) cases over the SW (SE and NE) regions for the strong warm phase SOI condition. For the strong cold phase SOI condition, the highest negative correlation coefficient values are found at the NWC region with lag-0 to lag-2 cases, and positive correlations are shown at the SW (SE and NE) regions with lag-0 and lag-2 (lag-1 to lag-3) cases. As a result, the stronger the warm and cold phases of ENSO forcing, the higher and lower the temperature with lag time 0 to 3 seasons over the USA.

5 Discussion

As shown in Figs. 5, 6, 7, 8, and 9, the results of this study show positive (negative) temperature response to the El Niño events at the NWC region (SW, SE, and NE regions) during

fall (0) to spring (+) seasons. Especially, the amplitude of the negative temperature departure of the El Niño year at the SW and SE regions is even higher than that of the non-El Niño year. On the contrary, during the cold phase of ENSO phenomena, the opposite patterns are detected (Figs. 10, 11, 12, 13, and 14). The monthly temperature indices are colder (warmer) than normal for the NWC (SW, SE, and NE) core region from fall (0) through spring (+) seasons. The amplitude of the positive temperature departure of the La Niña year at the SW region is much higher than that of the non-event year.

The opposite pattern of temperature anomalies over the northern and southern parts of the USA was documented in earlier studies (Cayan and Webb 1992; Emery and Hamilton 1985; Cayan and Peterson 1989) and was consistently shown in the relevant composites of the extreme phase of ENSO forcing. Spatial and temporal variation of cyclone over the Aleutian Islands and Gulf of Alaska is a prominent feature

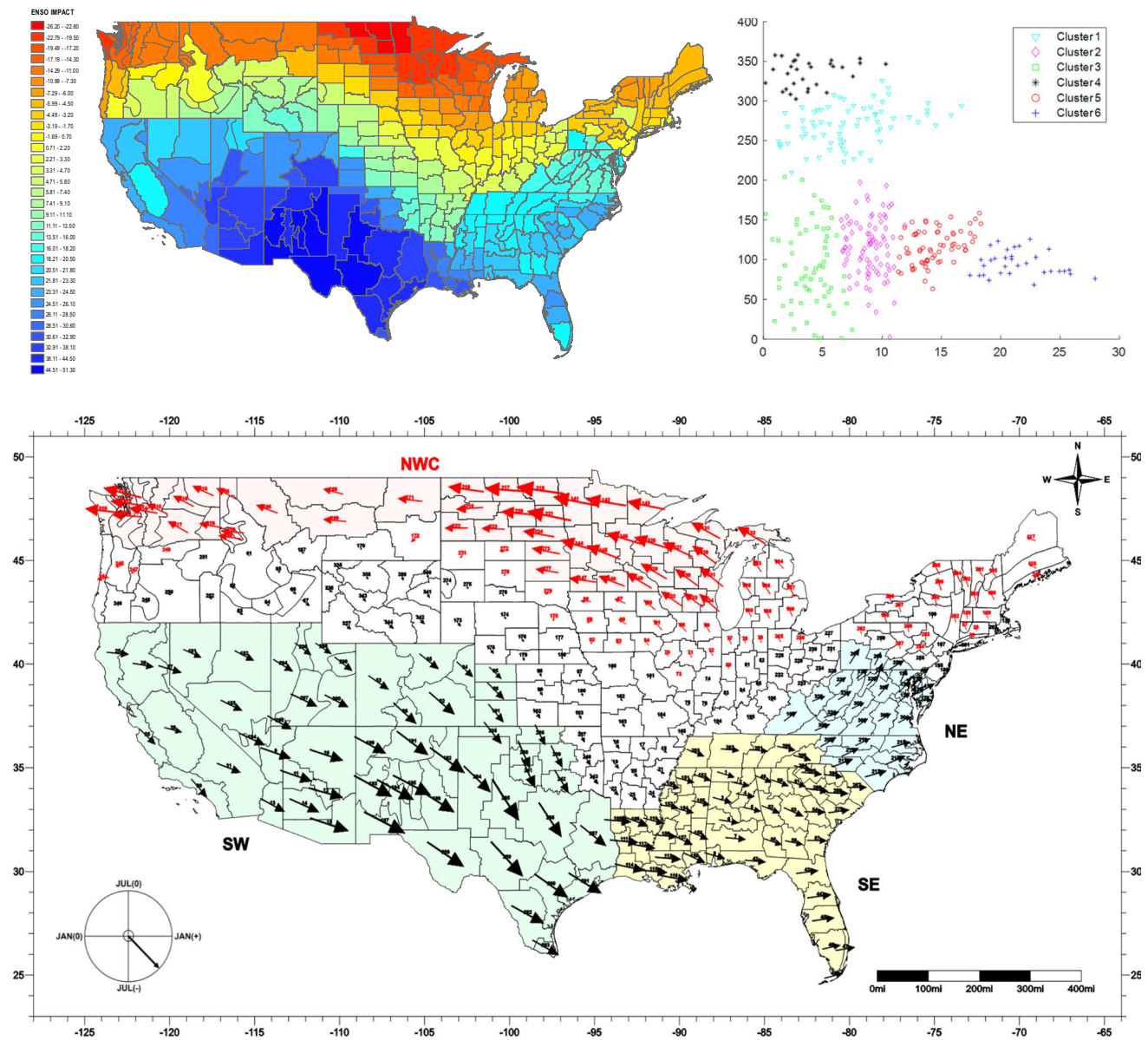


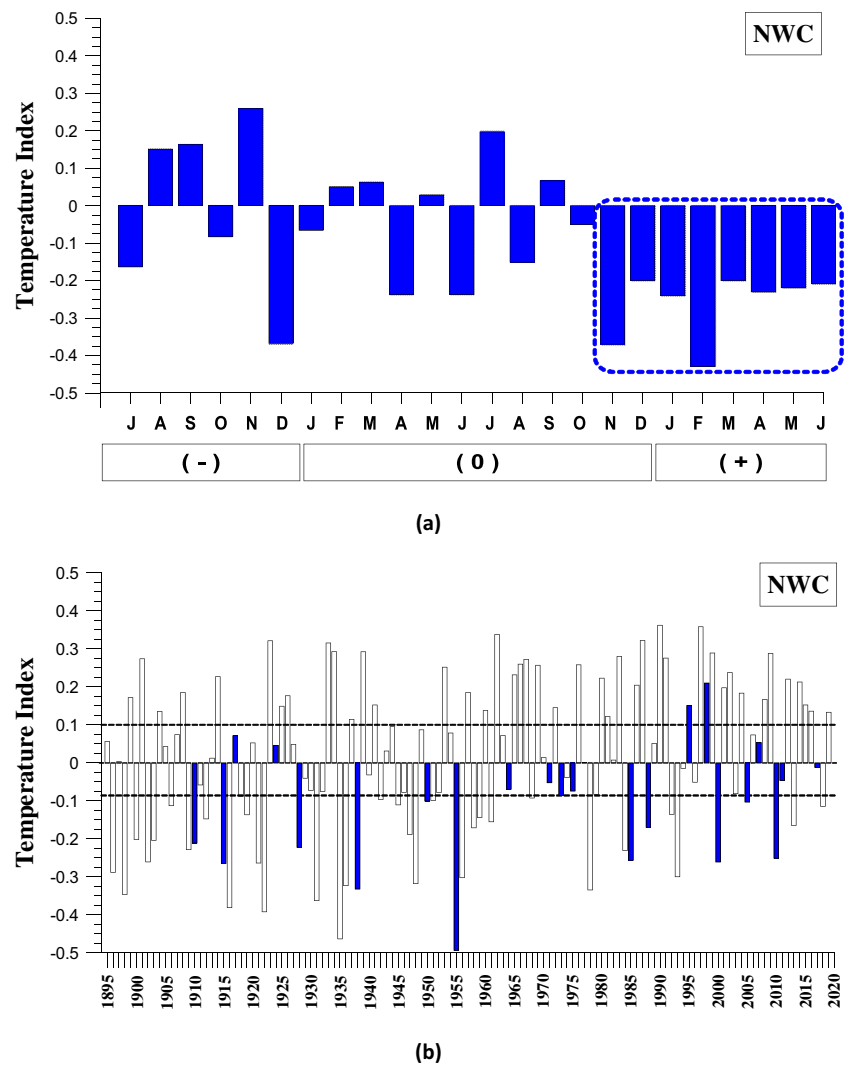
Fig. 10 Image map (upper left), clustering results (upper right), and harmonic dial map (lower) based on the first harmonic of the 2-year El Niño composites. In the image map, the blue areas indicate positive response of temperature anomalies to ENSO forcing, while the red areas indicate negative ENSO-related temperature signals. The

NWC region shows negative responses, while the SW, SE, and NE regions show positive responses. In the harmonic dial map, scale for the direction of arrows: south, July (–); west, January (0); north, July (0); and east, January (+). The magnitude of arrows is proportional with the amplitude of the harmonics

of climate patterns in the northeastern Pacific region. That is, the intensity and displacement of the Aleutian Low play an important role in featuring prominent Pacific climate variability on an annual basis. The intense cyclone brings relative warm seasons to the northern USA, while a weak cyclone favors cooler seasons. This cyclone’s variability comes from various sources but an important driver of the Aleutian Low pressure pattern is the large-scale fluctuation of sea surface temperature of tropical Pacific Ocean. The

warm phase of extreme ENSO events favors an especially intense cyclone related to the displacement of wind track in the eastern North Pacific. Seasonal wind patterns blow in a counterclockwise circulation over the Aleutian Low. As the shift moves southerly toward the northern USA, the condition favors a warm temperature. On the contrary, the cold phase of extreme ENSO events favors the opposite. During the cold events, the cyclone becomes weak and retreats to the northwest, while subtropical high-pressure pattern

Fig. 11 a La Niña aggregate composite for the candidate NWC region. The dashed line box delineates the season of possible La Niña-related responses. **b** The index time series for the NWC region for the season previously detected. La Niña years are shown by solid bars. The dashed horizontal lines are the upper (80%) and lower (20%) limits for the distribution of ITS values

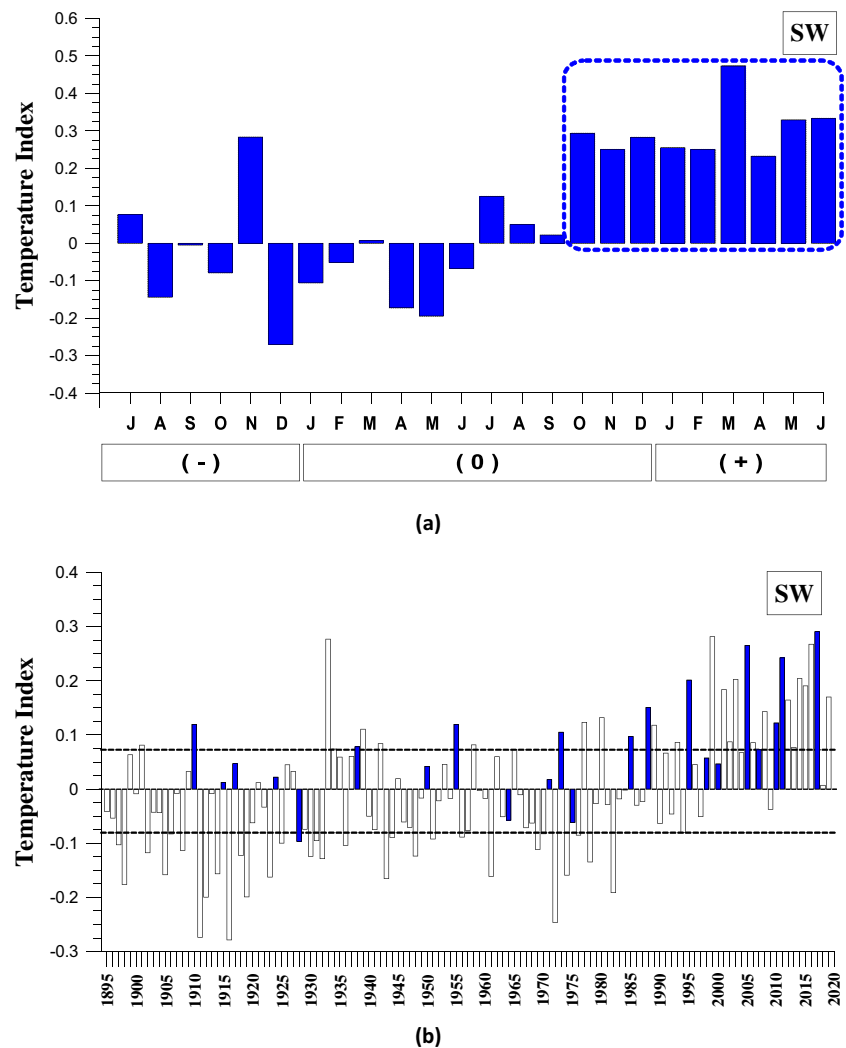


to the south displaces northward and intensifies. Surface winds blow in a clockwise circulation over a center of the anticyclone located offshore of southern California. Cayan and Webb (1992) stated that during the mature warm phase of ENSO phenomena in association with deepening of the Aleutian Island low pressure, the northward shift of the North Pacific storm paths causes warm conditions over the northern USA. On the other hand, the study by Emery and Hamilton (1985) showed that during the La Niña events, the depression of the cyclone, which is located over the Aleutian and Gulf of Alaska, modulates a more active low in the eastern Gulf of Alaska. These La Niña-related atmospheric activities affect the North Pacific winter storms shifting northward. As a result, cooler-than-average temperature patterns are observed over the northern part of the USA (Cayan and Peterson 1989).

The temperature response in the southern USA to the ENSO phenomena is consistent with Ropelewski

and Halpert (1986) and Douglas and Englehart (1981). Ropelewski and Halpert (1986) stated that the temperature response to ENSO may be more easily explained in terms of direct or shorter-range effects related to the enhanced subtropical jet stream and warmer-than-normal surface water over the Pacific. Rasmusson and Wallace (1983) found a strengthened subtropical jet stream displaced southward from its normal position during the mature phases of ENSO event (1982–1983). This pronounced intensification of the jet stream drove numerous winter storms causing cooling events in the southern parts of the USA. Additionally, they indicated that this region has shown abnormal cold conditions associated with past ENSO events. Douglas and Englehart (1981) suggested that the ENSO-related signal may be an indication of a more direct link to ENSO forcing than a Pacific North American teleconnection pattern (PNA). Active ENSO-related convection is typical in the equatorial Pacific, south of the southern USA. This convection has been linked

Fig. 12 As in Fig. 12, except for the candidate SW region

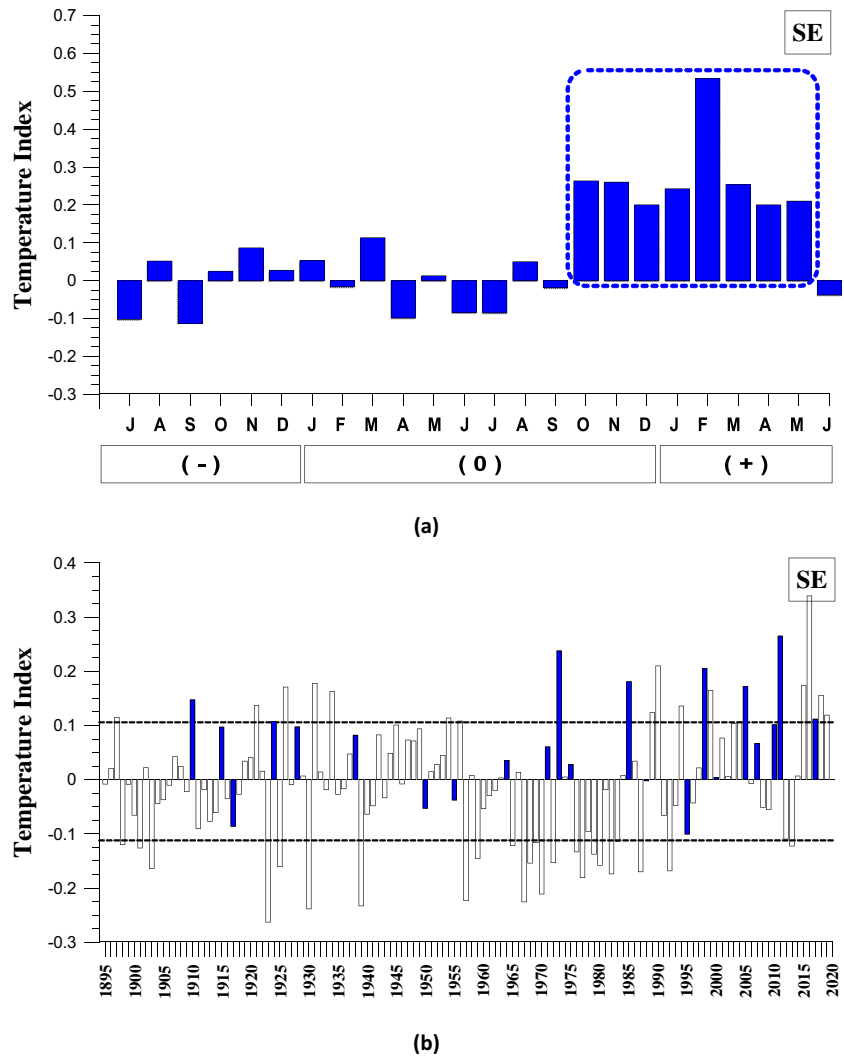


to stronger-than-normal westerlies in the southern parts of the USA including the Gulf of Mexico (e.g., 200 mb ENSO composites in Arkin 1982) and, hence, a tendency for more frequent cooling events in the southern USA. This possible direct link to the ENSO-related forcing may account for the consistent temperature response over the southern USA. During the ENSO event years, the persistent occurrence of warm/cold sea surface temperatures over the central and eastern equatorial Pacific triggers large-scale atmospheric fluctuations in the middle latitude based on complex air-sea coupled interactions. As a result, these ENSO-related middle latitude circulations excite abnormal temperature patterns over the USA. In addition, as shown in Figs. 5 and 10, stronger ENSO impacts on the eastern and southern US might be associated with ENSO causal effects on water cycle over these regions (Le et al. 2021; Le & Bae 2022).

6 Summary and conclusions

Teleconnection between two phases of ENSO thermal forcing and monthly temperature anomaly in the USA was investigated using a set of empirical and statistical analyses, such as harmonic analysis, annual cycle composites, and cross-correlation analysis. The details of the general results for ENSO-related temperature signals are outlined in Tables 2, 3, 4, and 5. From the results of vectorial mapping through composite and harmonic analyses, the proposed study area is classified into four core regions designated as the North-West/Central region (NWC), the South-West region (SW), the South-East region (SE), and the North-East region (NE). They showed high levels of spatial coherence and temporal consistency with notable spatial range and amplitude of

Fig. 13 As in Fig. 12, except for the candidate SE region



the temperature response to ENSO phenomena. The main conclusions are outlined as follows.

During the El Niño events, the monthly temperature anomalies are above normal in the NWC region and below normal in the SW, SE, and NE regions. For the NWC region, Nov (0) to May (+) is the signal season showing the noticeable consistency in temperature in association with the warm ENSO forcing, and Oct (0) to Apr (+), Nov (0) to May (+), and Oct (0) to Mar (+) are the signal seasons having a high level of temporal consistency in ENSO-related temperature responses for the SW, SE, and NE regions, respectively. The spatial coherence of the four core regions for the warm thermal forcing ranges from 0.93 to 0.99, and the temporal consistency is between 0.66 and 0.83. Especially, the SW core regions showed the highest magnitude of the

negative temperature departure for the El Niño years. For the La Niña events, the monthly temperature anomalies are below normal in NWC region and above normal in the SW, SE, and NE regions. The results of the composite and harmonic analyses show that the signal season for the cold period is Nov (0) to Jun (+) for the NWC region, and the signal seasons for warm periods are Oct (0) to Jun (+), Oct (0) to May (+), and Oct (0) to Mar (+) for the SW, SE, and NE regions, respectively. The spatial coherence rates for the four core regions for La Niña events range from 0.95 to 99, and the temporal consistency for each core region is 0.77 to 0.86.

Comparative analyses of temperature responses to both warm and cold ENSO events reveal the high significance level of the ENSO-temperature correlation with an opposite tendency in monthly temperature

Fig. 14 As in Fig. 12, except for the candidate NE region

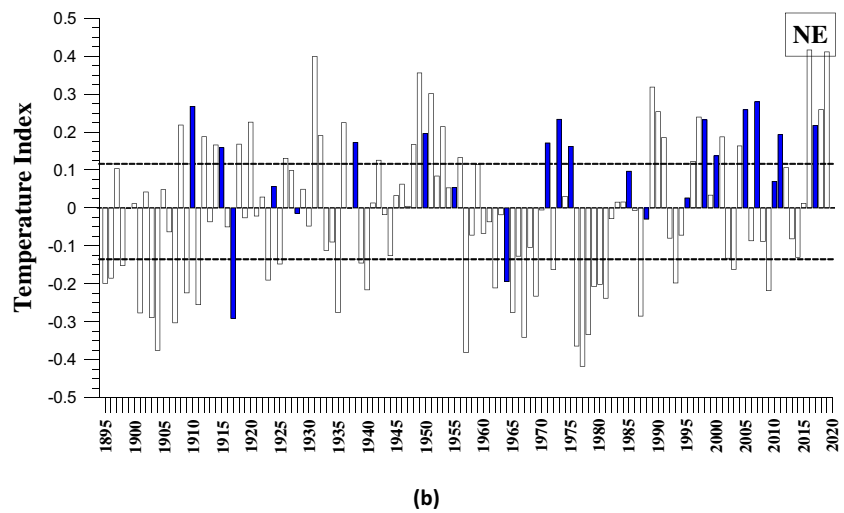
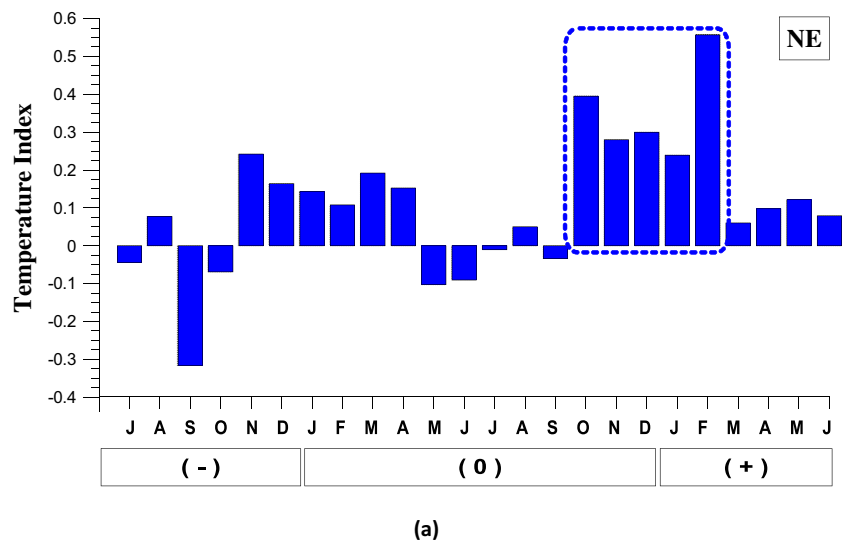


Table 3 Properties of the candidate regions (La Niña events)

Region	Season	Coherence	Total episode	Occurrence episode	Consistency	Extreme events
NWC	Nov (0)–Jun (+)	0.99	22	17	77%	8
SW	Oct (0)–Jun (+)	0.98	22	19	86%	10
SE	Oct (0)–May (+)	0.96	22	17	77%	8
NE	Oct (0)–Mar (+)	0.95	22	18	82%	8

Table 4 Probabilistic assessments for significance level based on the hypergeometric distribution (El Niño events)

Case	Region	<i>N</i>	<i>k</i>	<i>n</i>	<i>m</i>	Probability
I	NWC	125	63	29	24	0.000
	SW	125	65	29	21	0.004
	SE	125	62	29	21	0.008
	NE	125	59	29	19	0.040
II	NWC	125	25	25	13	0.000
	SW	125	25	25	13	0.000
	SE	125	25	25	10	0.008
	NE	125	25	25	8	0.085

Table 5 As in Table 4, except for La Niña events

Case	Region	<i>N</i>	<i>k</i>	<i>n</i>	<i>m</i>	Probability
I	NWC	125	65	22	17	0.003
	SW	125	63	22	19	0.000
	SE	125	61	22	17	0.005
	NE	125	66	22 <td 18	0.001	
II	NWC	125	25	22	8	0.039
	SW	125	25	22	10	0.003
	SE	125	25	22	8	0.039
	NE	125	25	22	8	0.039

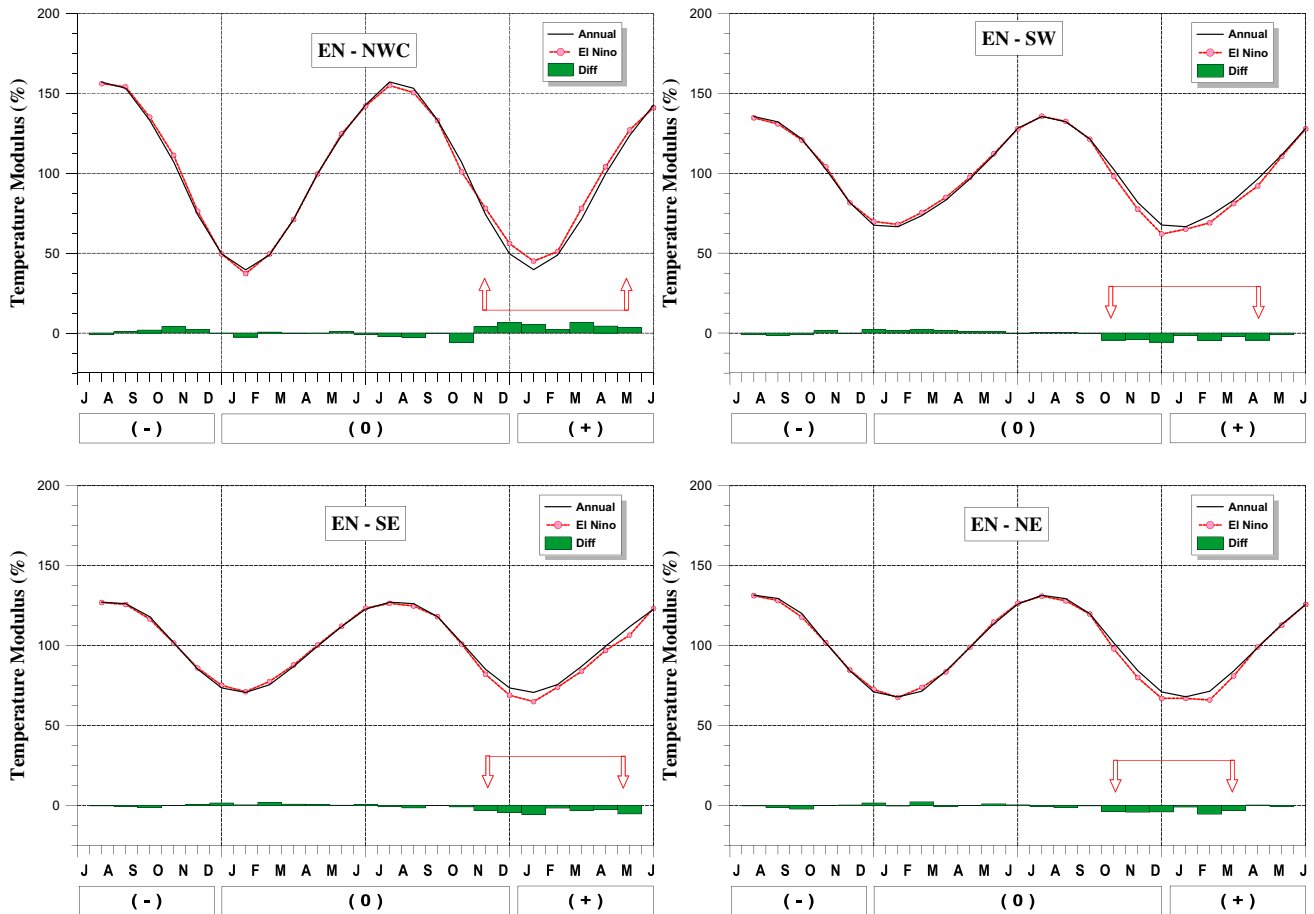


Fig. 15 The comparison between El Niño composite cycles (shown by dashed line) and annual cycles (shown by solid line) of the NWC, SW, SE, and NE regions, based on modular coefficients. Arrows indicate the beginning and end months of the ENSO signal season

anomalies. The NWC region shows positive (negative) tendency for warm (cold) phase, while the SW, SE, and NE regions show negative (positive) responses to the warm (cold) phase of ENSO episode. Below normal temperature anomalies during the El Niño thermal forcing are more significant than above normal temperature departures during the La Niña events. From the results of annual cycle analysis, the tropical heating and

cooling anomalies of sea surface temperature modulate the annual temperature cycle over the United States by increasing or decreasing. The highest positive (negative) correlation coefficient values are shown in the lag-0 to lag-2 cases for the NWC core region for the strong warm (cold) phase SOI condition. For the SW region, negative (positive) correlations are found in lag-0 to lag-2 cases for the strong warm (cold) phase

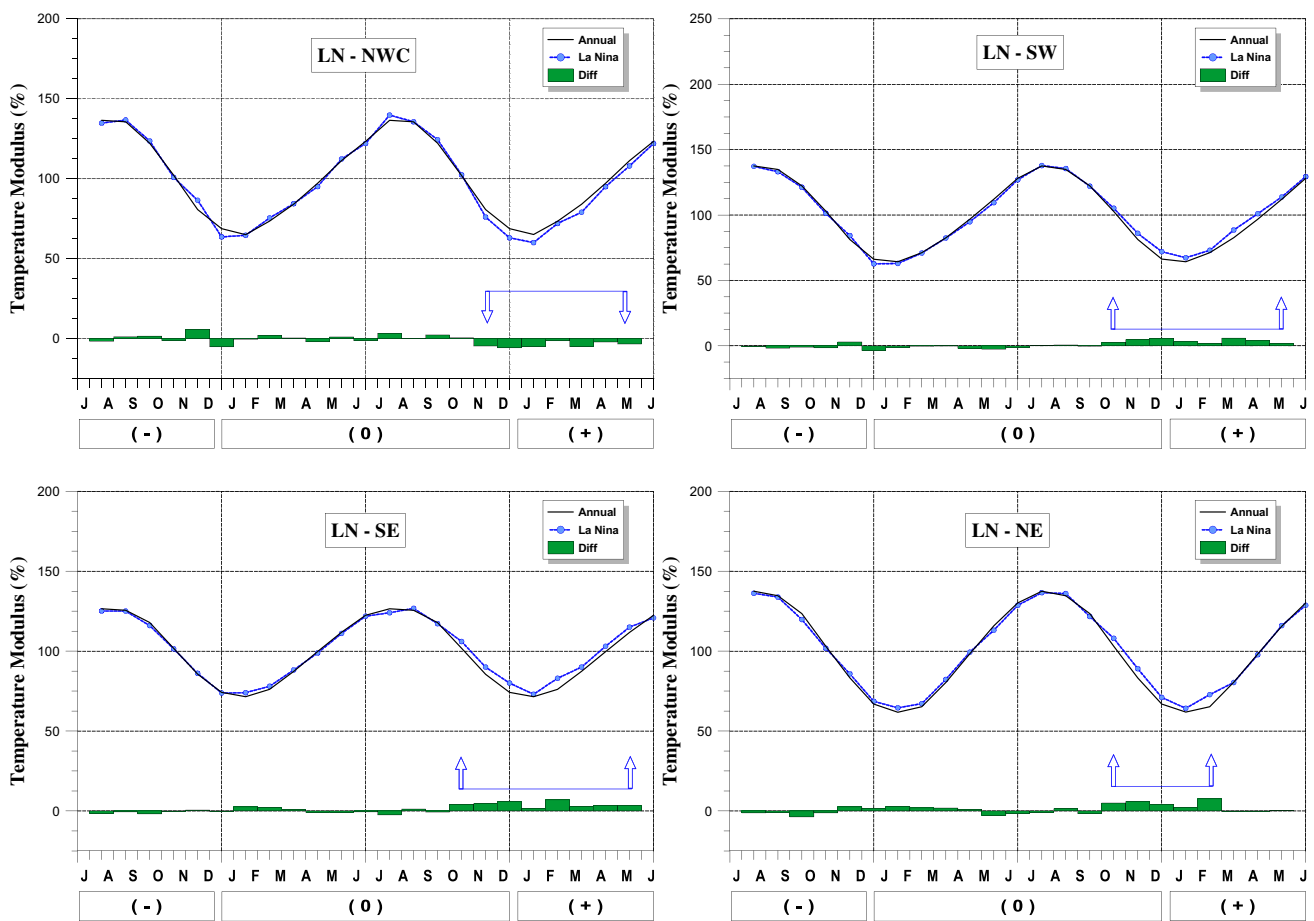


Fig. 16 As in Fig. 17, except for La Niña composite cycles

Table 6 Cross-correlation coefficients with respect to regions

Core region	Strong El Niño SOI					Normal condition					Strong La Niña SOI					
	Lag-0	Lag-1	Lag-2	Lag-3	Lag-4	Lag-0	Lag-1	Lag-2	Lag-3	Lag-4	Lag-0	Lag-1	Lag-2	Lag-3	Lag-4	
El Niño	NW	0.68	0.60	0.61	0.17	0.19	0.02	0.04	0.06	0.02	-0.05	-0.34	-0.35	-0.30	-0.03	-0.15
	SW	-0.47	-0.64	-0.72	0.00	-0.26	-0.17	-0.11	-0.08	-0.08	0.00	0.32	0.38	0.34	0.19	0.01
	SE	-0.21	-0.60	-0.62	-0.47	-0.18	-0.07	-0.10	0.00	-0.02	-0.02	0.14	0.42	0.24	0.52	-0.11
	NE	-0.08	-0.91	-0.80	-0.52	-0.17	-0.02	-0.05	0.00	-0.02	-0.05	-0.12	0.31	0.30	0.53	0.17
La Niña	NW	0.67	0.54	0.50	0.12	0.16	0.02	0.05	0.05	0.02	-0.04	-0.35	-0.38	-0.32	-0.04	-0.16
	SW	-0.45	-0.61	-0.52	0.09	0.12	-0.17	-0.11	-0.08	-0.06	0.04	0.33	0.41	0.38	0.28	0.13
	SE	-0.19	-0.52	-0.63	-0.45	-0.14	-0.05	-0.08	0.01	-0.01	-0.02	0.05	0.50	0.29	0.62	0.05
	NE	-0.20	-0.81	-0.74	-0.49	-0.21	0.02	-0.04	0.02	-0.01	-0.06	0.14	0.36	0.34	0.73	0.19

Bold values indicate statistically significant values

SOI condition and the same correlations are shown in lag-1 to lag-3 cases for the SE and NE regions. That is, the stronger the warm and cold phases of ENSO forcing, the more and less the temperature with lag time 0 to 3

seasons over the USA. From the findings above, it is concluded that middle-latitude temperature responses to the El Niño and La Niña phenomena are detectable over the contiguous USA.

Author contribution JL performed conceptualization, methodology, software, writing original draft preparation, investigation, and supervision. PJ contributed to conceptualization and validation of data and methodology. SL performed data curation and visualization.

Data availability Not applicable.

Code availability Not applicable.

Declarations

Ethics approval Not applicable.

Consent to participate Consent.

Consent for publication Consent.

Competing interests The authors declare no competing interests.

References

- Arkin PA (1982) The relationship between interannual variability in the 200 mb tropical wind field and the Southern Oscillation. *Mon Wea Rev* 110:1393–1404
- Berlage HP (1966) The Southern Oscillation and world weather. *Meteor Inst Meded Verh.* 88:152
- Bradley RS, Diaz HF, Kiladis GN, Eischeid JK (1987) ENSO signal in continental temperature and precipitation records. *Nature* 327:487–501
- Cayan DR, Webb RH (1992) El Niño/Southern Oscillation and streamflow in the western United States, in *El Niño: historical and paleoclimatic aspects of the Southern Oscillation*, edited by Diaz, H. F. and Markgraf, V., Cambridge University Press, 29–68.
- Cayan DR, Peterson DH (1989) The influence of North Pacific atmospheric circulation on streamflow in the West, in *Aspects of climate variability in the Pacific and the Western Americas*, Amer. Geophys Union, Monogr 55:375–397
- Daveyab MK, Brookshaw A, Inesona S (2014) The probability of the impact of ENSO on precipitation and near-surface temperature. *Clim Risk Manag* 1:5–24
- Douglas AE, Englehart PJ (1981) On a statistical relationship between autumn rainfall in the central equatorial Pacific and subsequent winter precipitation in Florida. *Mon Weather Rev* 109:2377–2382
- Emery WJ, Hamilton K (1985) Atmospheric forcing of interannual variability in the northeast Pacific Ocean: Connections with El Niño. *J Geophys Res* 90:857–868
- Haan CT (1977) *Statistical methods in hydrology*. Iowa State University Press, Ames, IA
- Halpert MS, Ropelewski CF (1992) Surface temperature patterns associated with the Southern Oscillation. *J Clim* 5:557–593
- Jin YH, Kawamura A, Jinno K, Berndtsson R (2005) Quantitative relationship between SOI and observed precipitation in southern Korea and Japan by nonparametric approaches. *J Hydrol* 301:54–65
- Kahya E, Dracup JA (1994) The influences of type 1 El Niño and La Niña events on streamflows in the Pacific southwest of the United States. *J Clim* 7:965–976
- Kemarau RA, Eboy OV (2022) The impact of El Niño–Southern Oscillation (ENSO) on temperature: a case study in Kuching, Sarawak, Malay J Soc Sci Humanit 6(1):289–297
- Kiladis GN, Diaz HF (1989a) Global climatic anomalies associated with extremes in the Southern Oscillation. *J Clim* 2:1069–1090
- Kiladis GN, Diaz HF (1989b) Global climatic anomalies associated with extremes in the Southern Oscillation. *J Clim* 2(9):1069–1090
- Kiladis GN, van Loon H (1988) The Southern Oscillation. Part VII: meteorological anomalies over the Indian and Pacific sectors associated with the extremes of the oscillation. *Mon Weather Rev* 116(1):120–136
- Le T, Ha KJ, Bae DH (2021) Projected response of global runoff to El Niño–Southern Oscillation. *Environ Res Lett* 16(8):084037
- Le T, Bae D (2022) Causal impacts of El Niño–Southern Oscillation on global soil moisture over the period 2015–2100. *Earth's Future*, 10(3).
- Lee JH, Julien PY (2016) Teleconnections of the ENSO and South Korean precipitation patterns. *J Hydrol* 534:237–250
- Lee JH, Julien PY (2017) ENSO impacts on temperature over South Korea. *Int J Climatol* 36(11):3651–3663
- Lee JH, Julien PY (2018) Influence of the El Niño/Southern Oscillation on streamflow variability. *Hydrol Process* 31(12):2162–2178
- Lee JH, Ramirez JA, Kim TW, Julien PY (2019a) Variability, teleconnection, and predictability of precipitation in relation to large scale climate indices. *J Hydrol* 568:12–25
- Lee JH, Julien PY, Maloney ED (2019b) The variability of temperature associated with climate indicators. *Theoret Appl Climatol* 138:469–489
- McKee TB, Doesken NJ, Kleist J (1993) The relationship of drought frequency and duration to time series. 8th Conference on Applied Climatology, Anaheim, CA 179–187.
- Rasmusson EM, Carpenter TH (1983) The relationship between eastern equatorial Pacific sea surface temperatures and rainfall over India and Sri Lanka. *Mon Wea Rev* 111:517–528
- Rasmusson EM, Wallace JM (1983) Meteorological aspects of the El Niño/southern oscillation. *Science* 222:1195–1202
- Redmond KT, Koch RW (1991) Surface climate and streamflow variability in the western United States and their relationship to large-scale circulation indices. *Water Resour Res* 27(9):2381–2399
- Ropelewski CF, Halpert MS (1986) North American precipitation and temperature patterns associated with El-Niño–Southern Oscillation (ENSO). *Mon Weather Rev* 114:2165–2352
- Ropelewski CF, Halpert MS (1987) Global and regional scale precipitation patterns associated with the El Niño/Southern Oscillation. *Mon Wea Rev* 115:1606–1626
- Ropelewski CF, Halpert MS (1989) Precipitation patterns associated with the high index phase of the Southern Oscillation. *J Clim* 2:268–284
- Tamaddun KA, Kalra A, Bernardez M, Ahmad S (2019) Effects of ENSO on temperature, precipitation, and potential evapotranspiration of North India's monsoon: an analysis of trend and entropy. *Water* 11(2):189
- van Loon H, Madden RA (1981) The Southern Oscillation Part I: global associations with pressure and temperature in northern winter. *Mon Weather Rev* 109(6):1150–1162
- Viet LV (2021) Development of a new ENSO index to assess the effects of ENSO on temperature over southern Vietnam. *Theoret Appl Climatol* 144:1119–1129
- Walker GT (1923) Correlation in seasonal variations of weather, V III, a preliminary study of world weather. *Mem Indian Meteorol Dep* 24:75–131
- Walker GT, Bliss EW (1932) World weather V. *Mem Roy Meteor Soc* 4(36):53–84
- Wilks DS (1995) *Statistical methods in atmospheric sciences*. Academic Press, 330–334.
- WMO (2014) *El Niño/Southern Oscillation*. WMO-No 1145:2–4

Publisher's note Springer Nature remains neutral with regard to jurisdictional claims in published maps and institutional affiliations.

Springer Nature or its licensor (e.g. a society or other partner) holds exclusive rights to this article under a publishing agreement with the author(s) or other rightsholder(s); author self-archiving of the accepted manuscript version of this article is solely governed by the terms of such publishing agreement and applicable law.